Matthias Rauterberg (Ed.)

Culture and Computing

8th International Conference, C&C 2020
Held as Part of the 22nd HCI International Conference, HCII 2020
Copenhagen, Denmark, July 19–24, 2020, Proceedings

HCI 2020
INTERNATIONAL

Springer

3D Virtual Reconstruction and Sound Simulation of an Ancient Roman Brass Musical Instrument

Zezhou Sun[1], Antonio Rodà[2(✉)], Emily Whiting[1], Emanuela Faresin[3], and Giuseppe Salemi[3]

[1] Computer Science Department, Boston University,
111 Cummington Mall, Boston, MA 02215, USA
{micou,whiting}@bu.edu

[2] Department of Information Engineering, University of Padova,
via Gradenigo 6b, 35131 Padova, Italy
roda@dei.unipd.it

[3] Deparment of Cultural Heritage, University of Padova,
Piazza Capitaniato 7, 35139 Padova, Italy
giuseppe.salemi@unipd.it

Abstract. Digital technologies based on 3D models are always more used to document archaeological remains and obtain hypothetical reconstructions when these remains are more or less heavily damaged. This work addresses the case of remains of ancient musical instruments, and in particular the case study of a brass instrument from the Roman Empire period, found in Voghenza (Italy). The pieces composing the instrument were first digitized by means of a structured light system, then virtually restored and recomposed applying a on-purpose developed algorithm. Finally, some sounds coherent with the geometry of the reconstructed model were simulated using a physically-based synthesis approach.

Keywords: 3D model · Virtual reconstruction · Sound simulation
musical cultural heritage

1 Introduction

For millennia, music culture has been handed down orally, since the first detailed written music documents are relatively recent [14]. Therefore, what we know about the music of the past is due to indirect documents, such as literature, music theory treatises, and iconography. In this context, archaeological finds of musical instruments such as ancient flutes or harps coming from ancient Egypt [1,2] or Greek-Roman areas are a very important direct source of information. Unfortunately, these instruments are often seriously damaged and cannot be played anymore. Therefore, observing these artefacts we can have an idea of the global shape and analyse the materials they are built from, but we can not listen to their sound and have experience of the performing practice.

Traditionally, playable copies of ancient instruments were built by craftsmen. This approach has several limits: a) the manufacturing process is usually slow and expensive; b) often one or few copies only can be built, limiting access to the instrument; c) when the reconstruction is uncertain, due to the poor state of conservation of the artefact, it is difficult to test and evaluate different possibilities.

The digital technologies based on 3D models overcomes these limits. The reconstruction is virtual, therefore many different hypotheses can be tested; FEM techniques [15] and physically informed algorithms allow to simulate the sounds produced by the artefacts, giving also a basis for evaluating the different reconstructions; virtual models can be easily shared, making possible global access to the heritage; finally, additive printing technologies offer the opportunity to have physical copies at relatively low costs. Nevertheless, methods and algorithms to obtain a virtual reconstruction of musical instruments in an automatic or semi-automatic way are still missing; several algorithms were developed in the past years for simulating the sound of known instruments, but these algorithms need to be modified and improved to meet the requirements of these ancient and almost unknown instruments; 3D printing processes need to be tuned to take into account the influence of materials and textures on the sound generation. These issues will be discussed and several solutions will be proposed in reference to the case study of an ancient Roman musical instrument, found in Voghenza, close to Ferrara (Italy) and now hosted in the archaeological section of the Civic Museum of Belriguardo. This instrument is the subject of an ongoing multidisciplinary project, that aims to analyse, reconstruct, and valorise this important musical heritage. A 3D model of the pieces composing the Voghenza instrument were first acquired and then subjected to two kinds of numerical elaboration. The first one aims to repair small holes and deformations, by means of filters and numerical interpolation, and is particularly suited for pieces with less severe damages. The second one aims to estimate the geometric parameters of the trumpet, also in case of very corrupted pieces. In particular, an original algorithm was developed to estimate the central axis of the curved tube of the trumpet and its increasing diameter.

2   3D Model

2.1   Acquisition

The trumpet, made of a metal alloy (probably bronze), is broken into 8 pieces and each piece further suffers from large holes and damages.

The 3d model of each piece was acquired by means of a structured light system that uses light patterns (or codes) and is based on digital cameras and projector. The projector shines a single pattern or a set of patterns onto the surface of an object; the camera then records the patterns on the surface. If the surface of the object under scanning is planar, then the pattern acquired by the camera would be similar to the pattern illuminated by the projector. However, if the object has some variations on the surface, the pattern acquired by the camera

would be distorted compared to the projector pattern. Therefore, the 3D shape of the object can be reconstructed by comparing the projected patterns acquired by the camera. The structured light systems have several advantages: they are fast, can be used for large areas, are able to reconstruct the geometry and to acquire texture of the 3D objects, at high resolution with high accuracy. However, they are sensitive to ambient illumination and they are also not suitable for scanning reflective and transparent surfaces [10]. The instrument used for the acquisition is Cronos Dual, a structured light system by Open Technologies, with an accuracy of 10–40 μm; camera resolution: 2 × 1.3 MPixels. The acquisition and post processing software is Optical RevEng 2.4 SR 8 Pro. In order to guarantee the better overlapping, an automatic turntable synchronized with the scanner was used. The rotation angle was set at 20° for each scan and 18 scans for set were made in order to complete the 360° rotation angle (Fig. 1).
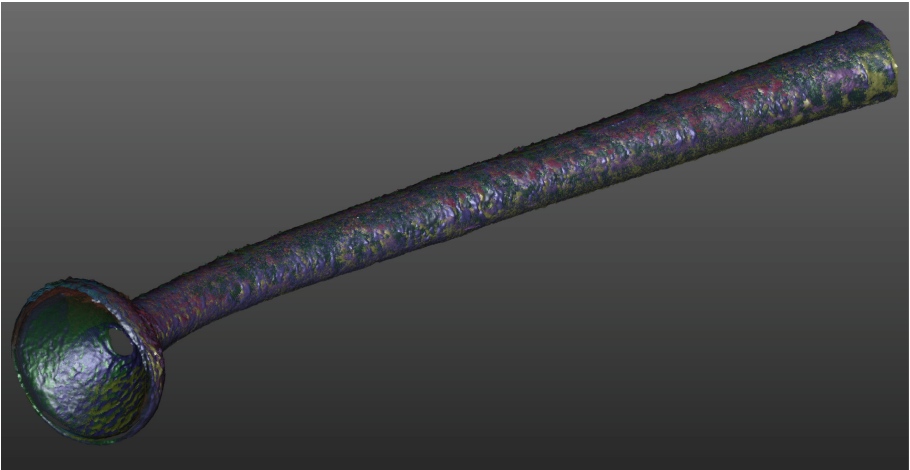

Fig. 1. The data collected by the scanner are X, Y, Z coordinate triplets of each single point acquired, taking a set of partially overlapping range scans. Different colours represent the contribution of each different scan. (Color figure online)

The pipeline of the processing phases is:

– Range map alignment: in order to put all the range maps into a common coordinate system where all the scans lie aligned on their mutual overlapping region. The pairwise ICP alignment algorithm, followed by a global registration, was used. An automatic pre-alignment technique was applied during the acquisition phase to improve this task and to verify, in real time, the acquisition quality.
– Range map merger (or fusion): to build a single, non-redundant triangulated mesh.

– Mesh editing: to improve the quality of the computed mesh. This step requires to order to correct the topological mistakes like cross section triangles or anomalous vertices.
– Mesh decimation: to accurately reduce the huge number of triangles, producing geometrically correct 3D models with different decimation factors (100%, 75%, 50% and 25%).
– Mesh export in STL (Standard Triangulation Language) format used for rapid prototyping in computer aided manufacturing.

2.2   Restoration

The two main tasks for restoration are to fix damaged areas and arrange the parts in the correct position and alignment. In previous work, Avanzini et al. [2] restored Pan flute damaged pipes by using cylinders generated from measurement. In our case, a difficulty is that the trumpet has non-uniform radius and curvature in 3D space. Hole filling for 3D scanning is a well studied field. Centil et al. [5] introduced a method to interpolate an implicit function obtained from a Poisson reconstruction which preserves the input mesh and the boundary curves. Liepa [11] proposed a procedure to interpolate the shape and density of the surrounding mesh to fill gaps. Both approaches achieve good performance in hole filling. But for our instrument model, severely damaged areas should not preserve boundaries. Example-based 3D scan completion [13] provides a high quality method to fill interior and large gap areas with the support of a dataset which contains many complete and similar objects. Dai et al. [8] proposes to complete the shape through a neural network classifier and a U-Net shape 3D-encoder-predictor through a well trained neural network. One challenge to apply these algorithms to our model is that we don't have a large dataset, and further, the arrangement of parts is not considered.

  Our restoration approach combines domain knowledge from archaeologists with 3D geometric analysis to find an estimation of its shape. A core assumption from archaeologists is the ordering of the eight broken parts, as labeled in Fig. 2. Observation from archaeologists on less damaged parts also tells us that the trumpet has a curved cylinder-like shape with elliptical cross-section and changing radius. Based on these insights, we developed a computational approach to automatically determine parameters of the elliptical cross-sections, as well as to estimate a central line that will aid in global alignment of the parts. Our pipeline (see Fig. 3) first estimates the central line of each part and performs part alignment. We then filter out less damaged areas and apply ellipse fittings. The final step is to reconstruct the complete instrument from the fitting result.

Estimate Central Line. We propose a computational method to align the individual parts into the global instrument shape. We compute an alignment based on estimating the central line of each individual part, assuming the instrument's central line lies on a plane.

  To get the central line for the instrument we used an iterative algorithm. We first place all mesh parts coarsely along the x-axis (see Fig. 4). We then

initialize k_i parallel cutting planes $P_j^{(i)}, j \in [1, k_i]$ (normal $(1,0,0)$) evenly spaced along the x-axis. Each cross-section is then given by $\psi_{ij} = \left\{ P_j^{(i)} \cap M_i \right\}$, where $M_i, i \in [1, 8]$ is the ith mesh part. Then Update ψ_{ij} by rotating them to XY plane, we simplified a 3D ellipse fitting to a 2D ellipse fitting problem. In 2D an ellipse can be expressed in general conic form
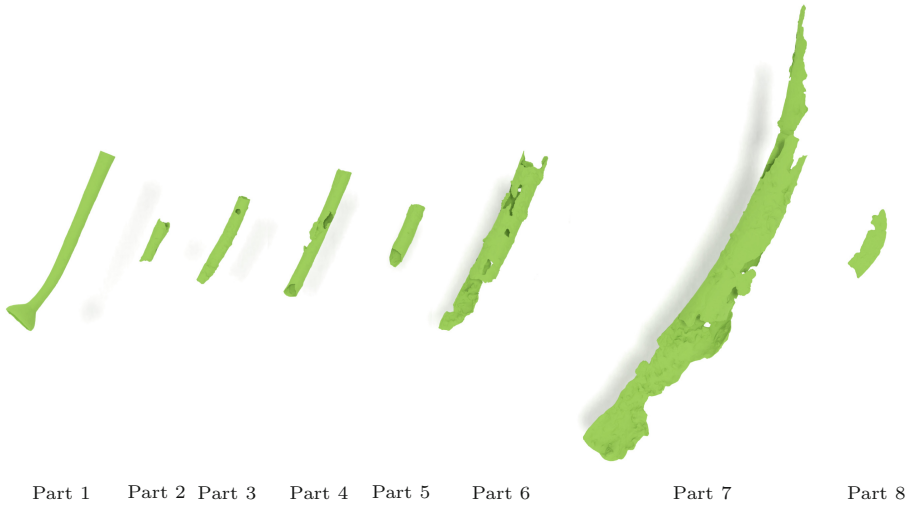

Part 1   Part 2 Part 3   Part 4   Part 5   Part 6   Part 7   Part 8

Fig. 2. Eight parts we get out of 3D scanning. From left to right are our part one to eight.

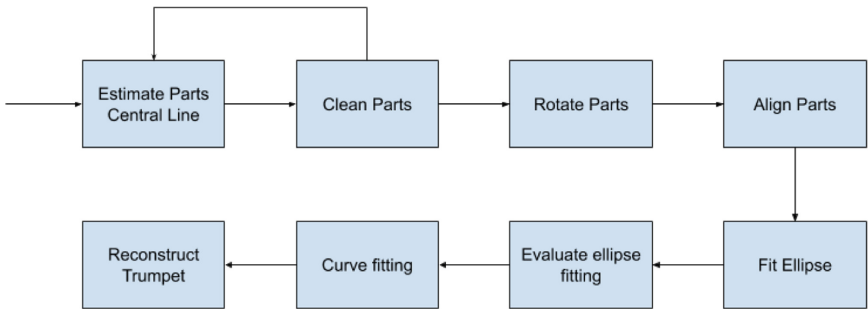**Fig. 3.** Our restoration pipeline

Fig. 4. All parts placed in order along x-axis.

$$D(X, a) = X \cdot \mathbf{a} = 0 \tag{1}$$

for $a_1^2 - 4a_0a_2 < 0$. Here, coefficient vector $\mathbf{a} = [a_0, a_1, a_2, a_3, a_4, a_5]^T$, and $X = [x^2, xy, y^2, x, y, 1]$. Then we need to minimize

$$\Gamma(a, \psi_{ij}) = \sum^{p \in \psi_{ij}} [D([p_x^2, p_x p_y, p_y^2, p_x, p_y, 1], \mathbf{a})]^2 \tag{2}$$

Let $n^{(i)} = |\psi_{ij}|$ be the number of points in ψ_{ij}, construct a $n^{(i)} \times 6$ matrix S and a 6×6 matrix A

$$S = \begin{bmatrix} x_1^2 & x_1 y_1 & y_1^2 & x_1 & y_1 & 1 \\ x_2^2 & x_2 y_2 & y_2^2 & x_2 & y_2 & 1 \\ \vdots & \vdots & \vdots & \vdots & \vdots & \vdots \\ x_{n^{(i)}}^2 & x_{n^{(i)}} y_{n^{(i)}} & y_{n^{(i)}}^2 & x_{n^{(i)}} & y_{n^{(i)}} & 1 \end{bmatrix}, A = \begin{bmatrix} 0 & 0 & 2 & 0 & 0 & 0 \\ 0 & -1 & 0 & 0 & 0 & 0 \\ 2 & 0 & 0 & 0 & 0 & 0 \\ 0 & 0 & 0 & 0 & 0 & 0 \\ 0 & 0 & 0 & 0 & 0 & 0 \\ 0 & 0 & 0 & 0 & 0 & 0 \end{bmatrix} \tag{3}$$

Then minimizing $\Gamma(a, \psi_{ij})$ is equivalent to minimizing $\|Sa\|^2$. The requirement of $a_1^2 - 4a_0a_2 < 0$ is not strong enough, so without loss of generality we can set the constraint $a_1^2 - 4a_0a_2 = -1$. Introducing Lagrange multiplier λ, we will get a best fit with largest λ where:

$$2S^T Sa - 2\lambda A\mathbf{a} = 0$$
$$\mathbf{a}^T A\mathbf{a} = 1 \tag{4}$$

Transformed to $\frac{1}{\lambda}\mathbf{a} = (S^T S)^{-1} A\mathbf{a}$, this can be solved as a standard eigenvalue problem. We will get best 2D ellipse fitting vector $a_{min,ij}$ for ψ_{ij} when we have smallest $\frac{1}{\lambda}$. Collect all centrals of fitted ellipses out of $a_{min,ij}$ and rotate them back to 3D space, we then have a collection of 3D points to estimate central line for each part $\left\{ c_j^{(i)} \right\}$.

Then in next iteration, we update cutting plane P_j^i to a plane passing through point $c_j^{(i)}$ and facing to $c_{j+1}^{(i)} - c_j^{(i)}$ and repeat steps above to get a new 3D point collection $\left\{ c_{new,j}^{(i)} \right\}$. Stop central line estimation if

$$\max \left\{ \|c_{new,j}^{(i)} - c_j^{(i)}\| \right\} \leq 0.5 \tag{5}$$

Otherwise let $c_j^{(i)} \leftarrow c_{new,j}^{(i)}$ and repeat this procedure.

We approximate our central lines for each part as $C_i = \left\{ c_{new,j}^{(i)} \right\}$. In our experiment, three iterations is enough to give a reliable central line estimation (Fig. 5).
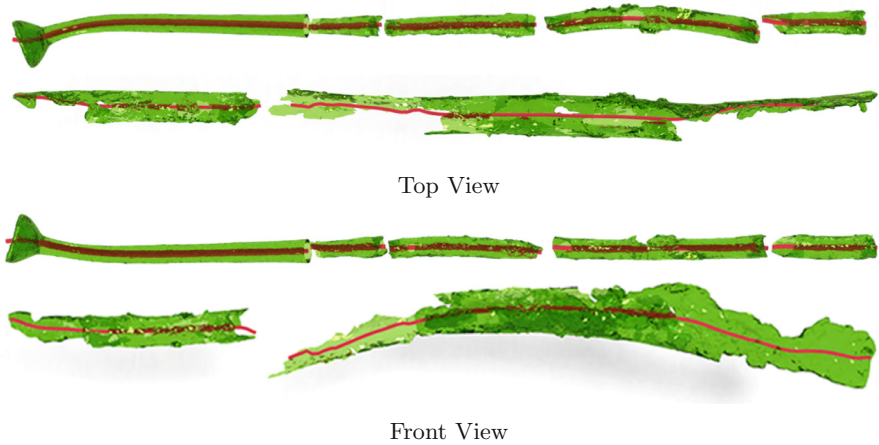
Top View

Front View

Fig. 5. Parts with estimated central lines (red) (Color figure online)

Clean Parts. 3D scanning is intended to scan the exterior surface area for each part. However, for severely damaged parts, the gaps expose interior surfaces during 3D scanning as well (yellow areas in Fig. 6). The difficulty is that the interior surfaces have a slightly smaller radius due to the thickness of the material, which leads to offsets in the ellipse fitting routine. We take an additional step to clean our meshes. For any triangle face f_n in M_i with centroid c_n, we define a condition

$$c_n \cdot \operatorname*{argmin}_{p \in C_i}(c_n - p)^2 > 0 \qquad (6)$$

If (6) stands, then face f_n belongs to the interior surface and is neglected. After removal of interior triangles for M_i, we filter out the region with the largest number of connected triangles through a flood-fill algorithm. We update our M_i to these cleaned parts and run the central line estimation to get our new C_i for each part.

Rotate Parts. Our part alignment approach consists of two steps: rotate parts to the same plane and align parts in 2D. In the rotation step, given an estimation of part's central line $C_i = \left\{ c_j^{(i)} = (c_{jx}^{(i)}, c_{jy}^{(i)}, c_{jz}^{(i)}), j \in [1, k_i] \right\}$, we want to find a best fit plane. We define a plane $b_0 x + b_1 y + b_2 z + b_3 = 0$ and denote $Q = (\frac{b_0}{b_2}, \frac{b_1}{b_2}, \frac{b_3}{b_2})^T$, $P_j = (c_{jx}^{(i)}, c_{jy}^{(i)}, 1)$. Then to find best fitting plane we minimize:

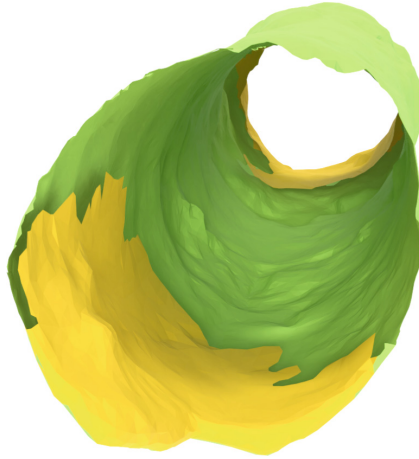$$E(Q) = \sum_{j}^{k_i} (c_{jz}^{(i)} - P_j Q)^2 \qquad (7)$$

Fig. 6. Interior surfaces are sometimes included in the 3D scan (yellow) when visible through gaps. This affects our fitting and needs to be removed. (Color figure online)

Let

$$
Y = \begin{pmatrix} c_{1z}^{(i)} \\ c_{2z}^{(i)} \\ \vdots \\ c_{k_i z}^{(i)} \end{pmatrix}, X = \begin{pmatrix} c_{1x}^{(i)} & c_{1y}^{(i)} & 1 \\ c_{2x}^{(i)} & c_{2y}^{(i)} & 1 \\ & \vdots & \\ c_{k_i x}^{(i)} & c_{k_i y}^{(i)} & 1 \end{pmatrix} \tag{8}
$$

For non-negative and convex function $E(Q)$, its minimum value locate at $\nabla E(Q) = [0,0,0]^T$. Then we get when $Q = (X^T X)^{-1} X^T Y$, we have minimum $E(Q)$. This Q will give us the best fit plane for central point samples.

After getting best fitting plane with normal vectors n_i for $C_i, i \in [1,8]$, we rotate mesh part $j \in [2,8]$ along axis $n_j \times n_1$ about angle $\arccos(n_j \cdot n_1)$ to make all parts lie on the same plane with part one. Then our alignment problem simplified to rotate mesh parts one the same plane.

Align Parts. After placing all parts on the same plane, our next step is to align them in order. We start at estimating each part starting and ending orientation. Orientation at any central line point $c_j^{(i)}$ is $c_{j+1}^{(i)} - c_j^{(i)}$ approximately. Then we apply Kriging algorithm [12], a Gaussian process regression to estimate orientation at starting point $c_1^{(i)}$ and ending point $c_{k_i}^{(i)}$. Denote the orientation at these two points as $o_1^{(i)}, o_{k_i}^{(i)}$. Once we get an estimation of parts orientations, for each M_i we use n_1 as rotation axis and rotate about $\arccos(o_1^{(i)} \cdot o_{k_i}^{(i-1)})$. Then translate it about $-c_1^{(j)} + c_{k_i}^{(j-1)}$ to align parts in order.

We call these new transformed mesh parts as M_i^* and all mesh parts together as M^*.

Fit Ellipse Along Central Line. After alignment of all parts, part i central point sample list will be transformed to C_i^*. Merge all these list in order we will get a new list C^*, which is a collection of points on an estimated central line for the entire instrument. With these points we can define $k*$ planes $\rho = \{P_1^*, P_2^*, ..., P_{k*}^*\}$, which are orthogonal to estimated central line and spaced evenly on it. Their intersections with mesh M^* will give us a collection of points collection: $\{\{P \cap M^*\} | P \in \rho\}$. Now we apply our 3D ellipse fitting algorithm to each points collection $\{P \cap M^*\}$, it will return us an ellipse central point collection $\lambda = \{(c_{xi}^*, c_{yi}^*, c_{zi}^*) | i \in [1, k*], i \in \mathbb{Z}\}$, a collection of semi-major axes $\mu = \{a_i^* | i \in [1, k*], i \in \mathbb{Z}\}$ and a collection of semi-minor axes $\nu = \{b_i^* | i \in [1, k*], i \in \mathbb{Z}\}$.

Evaluate Fitting. Considering that severely damaged areas will bring us biased ellipse fitting, we need to filter out them. An evaluation of fitting quality is required here. For cutting plane P_i^*, we know its intersection with mesh $\{P_i^* \cap M^*\}$ and its fitting ellipse is centered at $(c_{xi}^*, c_{yi}^*, c_{zi}^*)$ with semi-major axis a_i^* and semi-minor axis b_i^*. Let $d(p, (c_{xi}^*, c_{yi}^*, c_{zi}^*), a_i^*, b_i^*)$ be the shortest euclidean distance between point p to this fitting ellipse. We measure fitting quality through

$$Q(P_i^*) = \frac{\sum^{p \in \{P_i^* \cap M^*\}} d(p, (c_{xi}^*, c_{yi}^*, c_{zi}^*), a_i^*, b_i^*)}{|\{P_i^* \cap M^*\}|} \tag{9}$$

Computing $d(p, (c_{xi}^*, c_{yi}^*, c_{zi}^*), a_i^*, b_i^*)$ in 3D space is costly, but we can simplify it if transformed to 2D. Apply the same transformation which transforms ellipse to XY plane at origin with semi-major axis lay on X axis to both point and ellipse. Point p will be transformed to p^*. Because the symmetry of ellipse, we can transform point p^* to p' which is in the first quadrant by changing all its coordinate sign to positive, then solve for $t \in [-(b_i^*)^2, \infty]$ in

$$\left(\frac{a_i^* p_x'}{t + (a_i^*)^2}\right)^2 + \left(\frac{b_i^* p_y'}{t + (b_i^*)^2}\right)^2 - 1 = 0 \tag{10}$$

This will give us a point $(\frac{(a_i^*)^2 p_x'}{t+(a_i^*)^2}, \frac{(b_i^*)^2 p_y'}{t+(b_i^*)^2})$ on the ellipse whose distance to p' equals the shortest euclidean distance between $p*$ projection point on XY plane and the ellipse. This quartic equation can get an approximation root using iterative Newton method. To transform back to 3D space, we take p^*'s Z coordinate into consideration and compute Euclidean distance between p^* and closest point on ellipse, this is the shortest distance between p and ellipse in 3D space.

In the last step in this stage, for any plane P_i^*, if $Q(P_i^*) > 2.0$ we will filter out all corresponding ellipse fitting results in λ, μ, ν.

Curve Fitting. For every collection $\beta \in \{\mu, \nu\}$, we construct pairs $(c_{xi}^*, \beta_i), i \in [1, b], i \in \mathbb{Z}$, define a nonlinear model

$$H(x, (t_0, t_1, t_2)) = t_0 + t_1(x) + t_2(x)^2 \tag{11}$$

and define a function to minimize

$$G((t_0, t_1, t_2)) = \sum_i^{i \in [1, k^*]} [\beta_i - H(c^*_{xi}, (t_0, t_1, t_2))]^2 \tag{12}$$

We need to solve $\text{argmin}_{(t_0, t_1, t_2)} G((t_0, t_1, t_2))$. This is a curve fitting problem, where we apply the Levenberg–Marquardt algorithm.

Once we get a curve fitting minimized $G((t_0, t_1, t_2))$, we will generate a corresponding function $F(t), \mathbb{R} \to \mathbb{R}, t \in [\min(\{c^*_{xi}\}), \max(\{c^*_{xi}\})]$ to represent that fitting. For the central line, we apply the same curve fitting for each coordinate separately and combine the fitting result, giving $F_{central}(t), \mathbb{R} \to \mathbb{R}^3$ in the end. The fitting result for semi-major and semi-minor axes is plotted in Fig. 7.

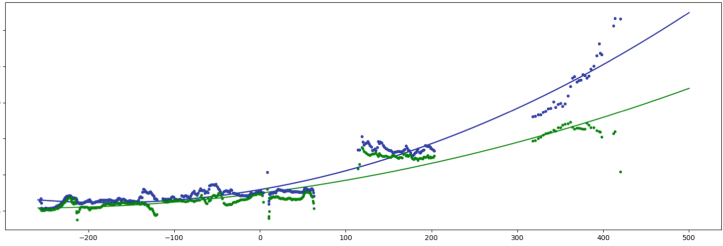**Fig. 7.** Semi-major axis and semi-minor axis fitting

Reconstruct Trumpet. After curve fitting, for parts 2 to 7 we acquire an explicit function $F_{central}(t), \mathbb{R} \to \mathbb{R}^3$ which gives us an estimation of their central line. $F_{major}(t), \mathbb{R} \to \mathbb{R}$ and $F_{minor}(t), \mathbb{R} \to \mathbb{R}$ represent an estimation of the semi-major and semi-minor axes of the corresponding fitted ellipse. Then for given $t \in [t_s, t_e]$, the instrument central line length can be computed as

$$L = \int_{t_s}^{t_e} \|F'_{central}(t)\| dt \tag{13}$$

At here we pick the t value where our have $F_{central}(t)_x = C^*_{x1}$ as t_s, and approximate central line length L on model. Then we can solve out our t_e by using Eq. 13.

Let t_i step through $[t_s, t_e]$ with constant interval t_c and $i \in [0, \frac{t_e - t_s}{t_c}]$. For every t_i, we first create ellipse points collection on XY plane.

$$\epsilon_i = \{(F_{major}(t_i) \cos(\theta), F_{minor}(t_i) \sin(\theta), 0) | \theta \in [0, 2\pi)\} \tag{14}$$

Let $D_i = normalize(F_{central}(t_{i+1}) - F_{central}(t_i))$, apply rotation to ϵ_i along axis $[0, 0, 1] \times D_i$ about angle $\arccos([0, 0, 1] \cdot D_i)$ and continue with translation $F_{central}(t)$, we will get ϵ^*_i. Construct triangles between ϵ^*_i and ϵ^*_{i+1} with $i \in [0, \frac{t_e - t_s}{t_c} - 1]$ and turn all triangles to mesh N^*, we will have an estimation of instrument part 2–7 exterior.

Our last step is to turn meshes with only exterior area to watertight meshes. We bring in Autodesk Meshmixer® to do rest job. Thickness of instrument can be measured at severe damaged area where both interior and exterior area are scanned and distance between them will give us an approximate thickness 1.2 mm. As for Part 1, it is preserved pretty well so we can use its 3D scanned mesh exterior as for final mesh generation directly. So we select exterior surface of M_1^* and N_* and applied 'offset' operation about '-1.2 mm' to generate watertight meshes. Generated mesh with aligned raw parts drawn at Fig. 8.

3   Sound Simulation

Having estimated the 3D model of the recomposed instrument, the aim of this section is to describe and simulate the set of tones that a musical instrument with that geometry can produce. The mouthpiece, very similar to that of modern trumpets, trombones and horns, reveals that the Voghenza instrument certainly belongs to the brass family. The modalities of sound generation of these instruments, that is how the acoustic waves are generated and propagate inside the cavity, are widely described in literature (e.g. [9]). From an acoustic point of view, brass instruments are generally divided in three parts: a mouthpiece, a cylindrical section, and a conical section ending with a more or less flared bell. The pitched sound is first generated by the lips that, leaning to the mouthpiece, are vibrated by the air emitted by the musician's respiratory system. The acoustic waves produced by the vibrating lips propagates through the cylindrical part, the length of which can be modified in many brass instruments by means of holes (as in the cornetto), valves (as in the trumpet) or a sliding mechanism (as in the trombone). Finally, the waves reach the ending flared section, where part of the acoustic energy is radiated to the outside the instrument and part is reflected inside the bore.

To what we can observe from the remains, the Voghenza instrument has no holes, valves or sliding parts, therefore the fundamental frequency of the tones that can be produced depend largely by the peaks of the acoustic impedance of the bore. This impedance can be estimated analytically, starting from the well known wave equation and solving it in the case of a wave propagating in a bore with an increasing diameter. The solution lets to the following Eq. [6] that allows the estimation of the frequencies f_n corresponding to a local maximum of the acoustic impedance:

$$f_n = \frac{c}{2(l + X_i)} \left[n - \frac{1 - \nu}{2} \right] \qquad (15)$$

where c is the sound speed propagation, l is the length of the cylindrical part, X_i is the length of the flared part, ν is a coefficient related to the shape of the flared part, and n is an integer number. To estimate the ν coefficient, the flared part is usually modeled by a Bessel function ([6,9]). In particular, being x the length of the central axis from the mouthpiece to a specific point of the bore, the radius of the bore is assumed to vary as a function of x according to the following equation:
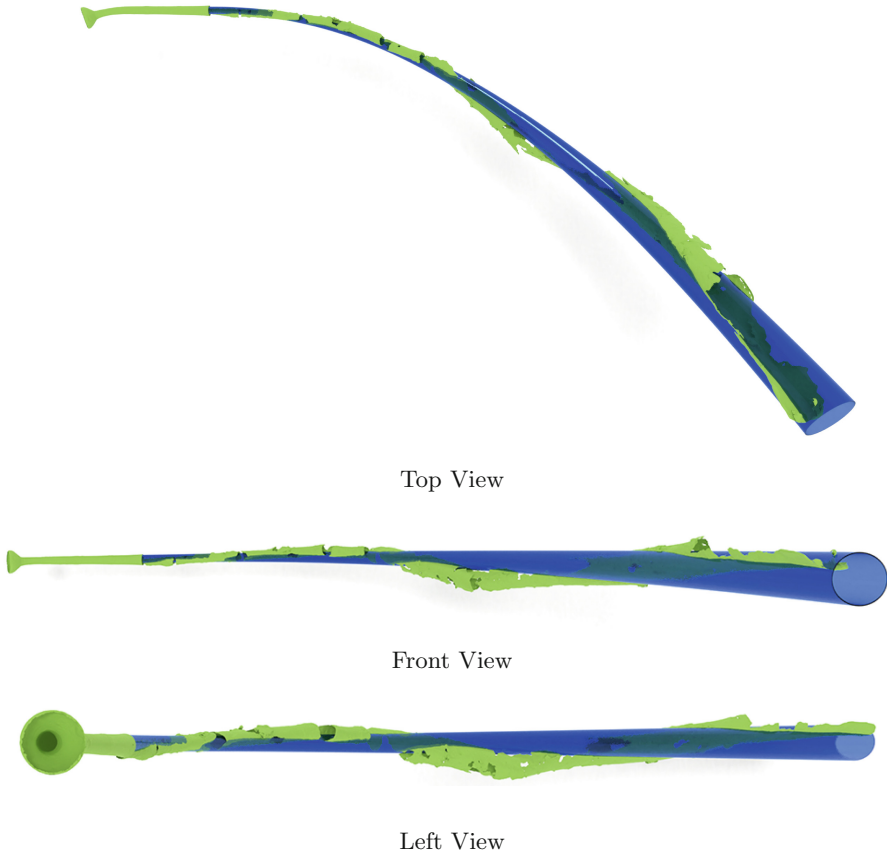
Top View

Front View

Left View

Fig. 8. Aligned trumpet parts from 3D scanning(green) and restored trumpet (blue) (Color figure online)

$$r(x) = \frac{b}{(x_a - x)^\nu} \tag{16}$$

where x_a is the distance between the end of the bore and the asymptote abscissa, b is a scale constant, and ν is a parameter that takes into account how rapidly the radius increases. The three unknown parameters of Eq. 16 were estimated fitting the geometry of the bore, as reconstructed in Sect. 2.2. Fitting the data obtained from the reconstructed model in a least-square sense ($R^2 = 0.91$, $df = 185$), we obtained the following values: $x_a = 1.3$, $b = 1000$, $\nu = 0.71$. Then, the frequencies of the natural resonance of the instrument ware estimated from Eq. 15 (see Table 1). Finally, a sample of these sounds[1] were generated by a physically-informed algorithm based on a waveguide model [7].

---

[1] Examples of the sounds can be listen at http://dei.unipd.it/~roda/brass.

Table 1. Natural resonant frequencies estimated by the geometry of the reconstructed 3D model of the instrument.

n	freq.[Hz]
1	123
2	266
3	409
4	553
5	696
6	839
7	982
8	1126
9	1269
10	1412

4   Conclusions

The 3D model of an ancient brass instrument was reconstructed starting from several partially damaged archaeological remains hosted in the Civic Museum of Belriguardo (Italy). The pieces were first digitized by means of a structured light system, then virtually restored and recomposed applying a on-purpose developed algorithm. Finally, some sounds coherent with the geometry of the reconstructed model were simulated using a physically-based synthesis approach. The results showed in this paper have several limitations that will be faced with further research and experimental work.

In restoration step, we assemble parts together based on estimated central line orientation at part ends and the approximation error of it in severely damaged area cannot neglect. The main reason of it is that least square based ellipse fitting don't perform very well in these areas. We can improve our restoration if change to a better ellipse fitting algorithm. Furthermore, for parts with nearly straight central lines, we neglected their rotation along central lines.

As concern the generated sounds, the Eq. 15 is only an approximated solution of the wave equation in an horn shaped bore and the approximation error increases for lower frequencies. We are going to evaluate this errors comparing the results with the ones obtained two methodologies: a) following a numerical approach based on the Finite Element Method; b) estimating the acoustic impedance of the bore by means of experimental measurements on a printed copy of the reconstructed model. Moreover, the sound simulation neglects at the moment the acoustic coupling with the player's mouth and all the aspects related to music performance, such as vibrato or amplitude envelope [3,4].

References

1. Avanzini, F., et al.: Virtual reconstruction of an ancient greek pan flute. In: Proceedings International Conference Sound and Music Computing (SMC 2016), pp. 41–46 (2016)
2. Avanzini, F., et al.: Archaeology and virtual acoustics. a pan flute from ancient Egypt. In: Proceedings of the 12th International Conference on Sound and Music Computing, pp. 31–36
3. Canazza, S., De Poli, G., Rodà, A.: Caro 2.0: an interactive system for expressive music rendering. Adv. Hum. Comput. Interact. **2015**, 1–13 (2015). https://doi.org/10.1155/2015/850474
4. Carnovalini, F., Roda, A.: A multilayered approach to automatic music generation and expressive performance, pp. 41–48 (2019). https://doi.org/10.1109/MMRP.2019.8665367
5. Centin, M., Pezzotti, N., Signoroni, A.: Poisson-driven seamless completion of triangular meshes. Comput. Aided Geometric Des. **35**, 42–55 (2015)
6. Chaigne, A., Kergomard, J.: Acoustics of Musical Instruments. Springer, New York (2016). https://doi.org/10.1007/978-1-4939-3679-3
7. Cook, P.: Tbone: an interactive waveguide brass instrument synthesis workbench for the NeXT machine. In: Proceedings International Computer Music Conference, pp. 297–299 (1991)
8. Dai, A., Ruizhongtai Qi, C., Nießner, M.: Shape completion using 3D-encoder-predictor CNNS and shape synthesis. In: Proceedings of the IEEE Conference on Computer Vision and Pattern Recognition, pp. 5868–5877 (2017)
9. Fletcher, N.H., Rossing, T.D.: The Physics of Musical Instruments. Springer, New York (2012). https://doi.org/10.1007/978-0-387-21603-4
10. Laga, H., Guo, Y., Tabia, H., Fisher, R.B., Bennamoun, M.: 3D Shape Analysis: Fundamentals, Theory and Applications. Wiley, Hoboken (2018)
11. Liepa, P.: Filling holes in meshes. In: Proceedings of the 2003 Eurographics/ACM SIGGRAPH Symposium on Geometry Processing, pp. 200–205 (2003)
12. Metheron, G.: Theory of regionalized variables and its applications. Cah. Centre Morrphol. Math. **5**, 211 (1971)
13. Pauly, M., Mitra, N.J., Giesen, J., Gross, M.H., Guibas, L.J.: Example-based 3D scan completion. In: Symposium on Geometry Processing, pp. 23–32 (2005)
14. Tomlinson, G.: Musicology, anthropology, history. In: The Cultural Study of Music, pp. 81–94. Routledge (2012)
15. Umetani, N., Panotopoulou, A., Schmidt, R., Whiting, E.: Printone: interactive resonance simulation for free-form print-wind instrument design. ACM Trans. Graph. **35**(6), 1–14 (2016). https://doi.org/10.1145/2980179.2980250. http://dl.acm.org/citation.cfm?doid=2980179.2980250